Published in final edited form as:
Cancer Res. 2010 March 15; 70(6): 2224–2234. doi:10.1158/0008-5472.CAN-09-3515.

Matrix Metalloproteinases Contribute Distinct Roles in Neuroendocrine Prostate Carcinogenesis, Metastasis, and Angiogenesis Progression

Laurie E. Littlepage[1], **Mark D. Sternlicht**[1,4], **Nathalie Rougier**[1,5], **Joanna Phillips**[1], **Eugenio Gallo**[1], **Ying Yu**[1], **Kurt Williams**[2], **Audrey Brenot**[1], **Jeffrey I. Gordon**[3], and **Zena Werb**[1]

[1]Department of Anatomy, University of California, San Francisco, CA 94143-0452

[2]VisEn Medical, Inc., 45 Wiggins, Bedford, MA 01730

[3]Center for Genome Sciences, Washington University School of Medicine, St. Louis, MO 63108

Abstract

Prostate cancer is the leading form of cancer in men. Prostate tumors often contain neuroendocrine differentiation, which correlates with androgen-independent progression and poor prognosis. Matrix metalloproteinases (MMPs), a family of enzymes that remodel the microenvironment, are associated with tumorigenesis and metastasis. To evaluate MMPs during metastatic prostatic neuroendocrine cancer development, we used transgenic mice expressing SV40 large T antigen in their prostatic neuroendocrine cells, under the control of transcriptional regulatory elements from the mouse cryptdin-2 gene (CR2-TAg). These mice have a stereotypical pattern of tumorigenesis and metastasis. MMP-2, -7, and -9 activities increased concurrently with the transition to invasive metastatic carcinoma, but they were expressed in different prostatic cell types: stromal, luminal epithelium, and macrophages, respectively. CR2-TAg mice treated with AG3340/Prinomastat, an MMP inhibitor that blocks activity of MMP-2, -9, -13, and −14, had reduced tumor burden. CR2-TAg animals were crossed to mice homozygous for null alleles of MMP-2, -7, or -9 genes. At 24 weeks CR2-TAg; MMP-2$^{-/-}$ mice showed reduced tumor burden, prolonged survival, decreased lung metastasis, and decreased blood vessel density, whereas deficiencies in MMP-7 or MMP-9 did not influence tumor growth or survival. Mice deficient for MMP-7 had reduced endothelial area coverage and decreased vessel size, and mice lacking MMP-9 had increased numbers of invasive foci and increased perivascular invasion as well as decreased tumor blood vessel size. Together these results suggest distinct contributions by MMPs to the progression of aggressive prostate tumor and to helping tumors cleverly find alternative routes to malignant progression.

Introduction

In men, prostate cancer is the most diagnosed cancer and is second only to lung cancer in cancer deaths in the USA (1). Most human prostate carcinomas respond to hormonal therapy initially but often become more aggressive and hormone refractory. Most adenocarcinomas contain foci marked by a characteristic neuroendocrine-like differentiation (NED) pattern (2-4). These

Address all correspondence to: Zena Werb, Department of Anatomy, University of California, San Francisco, CA 94143-0452, Tel: (415) 476-4622 (office), Fax: (415) 476-4565, Tel: (415) 476-4758 (Laboratory), zena.werb@ucsf.edu.
[4]Present address: FibroGen, 409 Illinois St., San Francisco, CA 94158
[5]Present address: Hôpital Bichat-Claude-Bernard, 46, rue Henri-Huchard, 75018 Paris, France

Disclosure of Potential Conflicts of Interest: K.W. is an employee of VisEn Medical, Inc. The other authors disclosed no conflicts of interest.

foci do not express the androgen receptor and are considered androgen-insensitive (5). As prostate tumors progress, their histopathology may exhibit increased NED with associated androgen-independence (6). Increased levels of NED biomarkers correlate with increased tumor progression, refractoriness to hormone-based regimens, and poor prognosis (4,7). However, little is known about the factors regulating growth of these NED-positive tumors.

CR2-TAg transgenic mice express simian virus 40 tumor antigen (SV40 TAg), under the control of transcriptional regulatory elements from the cryptidin-2 gene, in a subset of neuroendocrine cells present in the prostate (8,9). By eight weeks of age, prostatic intraepithelial neoplasia (PIN) lesions are evident. Focal invasion begins at 10-12 weeks, and visible tumors are formed by around 16 weeks. 100% of these mice develop prostate tumors by 24 weeks, with the majority exhibiting metastases to peripheral tissues, including lung, liver, lymph nodes, and bone. The tumor is characterized by cells with a high nuclear to cytoplasmic volume ratio and abundant rosette formation characteristic of a neuroendocrine tumor. The neoplastic cells in CR2-TAg mice express neuroendocrine markers, are androgen receptor-negative, and demonstrate androgen independence.

Matrix metalloproteinases (MMPs) are a family of enzymes that cleave a broad range of components of the extracellular matrix (ECM), basement membrane, growth factors, and cell surface receptors (10,11). MMPs are upregulated in cancer progression, can act as oncogenes, and promote invasion and metastasis in virtually all solid tumors (10,11). These enzymes play a role not only in tumor initiation and invasion but also in angiogenesis, metastasis and in releasing other tumor-promoting factors. Stromal and inflammatory cells, rather than tumor cells, typically synthesize MMPs, which can then act on the stroma and regulate the tumor microenvironment as well as acting on tumor cells themselves (10,11).

Several MMPs are overexpressed in prostate cancer progression, and androgen ablation or castration increases levels of MMPs (12-15). Indeed, increased expression of MMP-2 in cancer cells is an independent predictor of decreased prostate cancer disease-free survival (16). Moreover, a synthetic inhibitor of MMPs decreases tumor growth and metastases in a rat prostate cancer model (17), and reduced expression of MMP-9 in prostatic carcinoma cells results in reduced lung metastases but does not affect the tumor growth rate (18).

The high penetrance of tumor progression makes the CR2-TAg mouse an attractive model for characterizing the contribution of MMPs to aggressive neuroendocrine tumor progression. Therefore, in this study we used both pharmacological and genetic approaches to determine the effect of MMP-2, -7, and -9, on the progression of carcinogenesis, metastasis, and angiogenesis.

Materials and Methods

Transgenic mouse models

Mice homozygous for null alleles of the MMP-2 (19), MMP-7 (20), MMP-9 (21), and CR2-TAg transgene (8,9) were genotyped using published protocols. All were backcrossed to FVB/N in the UCSF mouse tumor model core. Mice were maintained under pathogen-free conditions in the UCSF barrier facility. All animal protocols were reviewed and approved by the UCSF Institution Animal Care and Use Committee.

Detection of MMP activity

Two nmol of MMPSense molecular imaging agent (VisEn Medical Inc., Bedford, Massachusetts) was injected into the tail vein of mice 12-18 hours prior to imaging (22,23). Mice used in Figure 1 were CR2-TAg;MMP-$7^{+/-}$ or MMP-$7^{+/+}$. All tomographic studies were performed using VisEn's fluorescence molecular tomography (FMT1) system. Fluorochrome

quantification was determined by establishing three-dimensional regions of interest (ROIs). Fluorochrome concentration was calculated automatically from the reconstructed images using FMT1 Imaging Software in the context of pre-acquired calibrations. Data are expressed as pmol fluorescence per ROI.

Gelatin zymography was performed as described previously (24). For MMP-7 western blots, we loaded 30 μg of protein per lane, as determined by Bradford protein assay (Bio-Rad), on NuPAGE 4-12% Bis-Tris gradient gels with MES running buffer (Invitrogen) and used goat anti-mouse MMP-7 (R&D Systems) at a dilution of 1:500 in 3% milk prepared in PBS with 0.1% Tween. Chemiluminescence was detected using a Fujifilm ImageQuant LAS-4000, and relative intensity of bands was quantified using Photoshop to calculate intensities relative to actin levels.

Tissue collection

The prostate lobes were removed, weighed, fixed in 4% paraformaldehyde overnight, and stored embedded in paraffin or frozen in OCT until sectioning. Lung, liver, lymph node and bone were collected and processed similarly to the prostate tissue. Bones were decalcified in EDTA following fixation.

Immunohistochemistry

All antibodies and conditions used for immunostaining of tissues in this study are listed in Supplemental Table 1. We used the following antibodies: anti-MMP-2 (Cell Signaling), anti-MMP-2 (Chemicon), anti-MMP-7 (R&D Systems) and (25), MMP-9 (26), anti-phosphohistone H3 (Cell Signaling), anti-cleaved caspase-3 (Cell Signaling), anti-CD31 (Pharmingen), anti-α–smooth muscle actin Clone 1A4 Cy3 conjugate (Sigma), anti-F4/80 (Caltag), anti-CD45 (BD Pharmingen), anti-synaptophysin (DAKO), rabbit anti-SV40-TAg (gift of Dr. Doug Hanahan), biotinylated anti-rabbit and anti-rat IgG (Vector), Alexa 488, 568 594 anti-rat or anti-rabbit secondary antibodies (Molecular Probes), peroxidase-conjugated anti-rat IgG (Jackson ImmunoResearch).

We cut 20 μm sections for vasculature staining from frozen blocks and usually 5 μm sections from paraffin-embedded blocks for hematoxylin and eosin (H&E) staining and immunocytochemistry. Images were captured using a Leica DMR microscope.

Tumor pathological grading

For tumor samples harvested from 24-week-old animals, tissue sections were stained by H&E and given a score of 1-3, where 1=“PIN” (more than 60% of tissue is PIN and normal glands), 2=“Mixed” (40-60% PIN, 40-60% Carcinoma), or 3=“Carcinoma” (more than 60% of tissue is carcinoma). Mouse prostate pathology terms used follow the Bar Harbor classification system (27). For 16-week prostate tissue samples, H&E-stained sections were scored blinded by a trained pathologist for the glands containing invasive foci as a percentage of total glands.

Pharmacological intervention

AG3340/Prinomastat (28) was provided by David Shalinsky (Agouron Pharmaceuticals, La Jolla, CA). The inhibitor was prepared at 3 mg/ml in acidified drinking water, pH 2.3, and filter sterilized. Mice received the drug orally *ad libitum* beginning at six weeks of age, changed every two weeks, and continued until tissues were harvested at 24 weeks. Control mice received the same volume of acidified drinking water without inhibitor.

Metastasis analysis

Harvested lung and liver were immediately scored for visible surface-associated macro-metastatic (macromet) nodules and then processed. H&E stained sections were scored for micro-metastases (micromets). For each mouse, one section was analyzed initially. If metastasis was not detected, then two to six more sections were analyzed per mouse.

Quantification of vasculature and tumor cell invasion

For vessel density, vasculature was counted manually from sections stained for CD31 and SMA. We defined a pericyte-covered vessel as a $CD31^+$ vessel with at least one surrounding SMA^+ cell. Vasculature area was quantified using Image J 1.38× (National Institutes of Health). Average vessel size was calculated by dividing the vasculature area by vessel density. Tumor cell invasion was scored for SV40 TAg positive stromal cells associated with vasculature (perivascular invasion) or cells not associated with vasculature (infiltrative invasion) as a percentage of total invasive cells (i.e., number of perivascular + infiltrative invasive cells).

Statistical analysis

Kaplan-Meier survival curves were analyzed by Logrank tests to determine the significance of observed differences between the curves. Metastases were analyzed by Fisher's Exact test. Median tumor weights and invasive status (perivascular or infiltrative) were compared using Mann-Whitney tests. Statistical analysis other than for metastases used Prism 4 software (GraphPad Software, Inc.). All cohorts composed of three or more genotypes were compared using one-way analysis of variance (ANOVA) and using unpaired Student's t tests for comparing two cohorts. In all experiments, $p < 0.05$ was considered statistically significant.

Results

MMP activities increase during CR2-TAg prostate tumor progression

We first analyzed MMP activity in the CR2-TAg model using MMP substrate-based tomography. CR2-TAg transgenic mice and nontransgenic controls were injected with a pan-MMP probe, MMPSense, that becomes fluorescent following cleavage by active MMPs, including MMP-2, -3, -9, and -13 (22,23). Noninvasive whole body optical tomography indicated that CR2-TAg mice had significantly increased MMP activity in the region of their prostate compared to non-transgenic littermates ($p=0.004$; Student's t test; Fig. 1A).

By gelatin zymography, we found no significant difference in MMP-2 activity at 16 and 24 weeks of age in non-transgenic littermate prostate samples (Fig. 1B). At 16 weeks (local microinvasion stage), dorsolateral prostate samples from CR2-TAg mice had increased levels of active MMP-2, pro-MMP-9 and active MMP-9. By 24 weeks, when 100% of the CR2-TAg mice have tumors and the majority have liver metastases (9), active MMP-2 and MMP-9 levels were significantly increased in the prostate, seminal vesicles (marker of local prostate cancer invasion) and liver (frequent site of metastasis).

Western blot analyses revealed increased levels of active MMP-7 by 12 weeks in CR2-TAg prostates, with variable activity at 24 weeks (Fig, 1B).

MMP-2 and MMP-9 localizes to stromal cells, whereas MMP-7 localizes to a subclass of luminal cells

Prostatic stromal cells may be involved in progression of prostate adenocarcinomas (29,30). These previous studies suggest that increased MMP-2 and MMP-9 levels reflect stromal cells, rather than tumor epithelial cell, contributions (10).

MMP-2 localized to the stroma within and surrounding the CR2-TAg tumors and co-localized with F4/80 (macrophage marker) and α-smooth muscle actin (SMA, a marker of stromal carcinoma-associated fibroblasts, pericytes, and smooth muscle cells) at 24 weeks (Fig. 1C, D). MMP-9 localized to the stroma surrounding the tumor and in stromal regions within the tumor itself (Fig. 1C, Supplemental Fig. 1A, B), often adjacent to clusters of malignant cells and in regions enriched for blood vessels and stroma. MMP-9 was prominent in macrophages, detected by co-staining with anti-F4/80 (Fig. 1D). Therefore, MMP-2 and MMP-9 reside in stromal rather than epithelial cells.

The prostate contains three epithelial cell types: luminal secretory cells, basal cells found between the luminal cells and basement membrane, and scattered neuroendocrine cells. We observed MMP-7 staining at the apical surface of infrequent luminal cells located in normal prostate as well as in abnormal neoplastic glands from 16-week-old CR2-TAg mice (Supplemental Fig.1C, D). MMP-7 did not colocalize with the neuroendocrine cell marker synaptophysin by immunofluorescence, indicating that MMP-7 positive cells are not likely from the neuroendocrine lineage (Supplemental Fig. 1E). By 24 weeks of age, MMP-7 was visible in non-neoplastic prostatic glandular tissue, but not within the tumor itself (Fig. 1C), similar to its localization in normal mouse and rat prostate and in human tumors of the breast and colon (25, 31).

MMP inhibitor AG3340 increases survival and decreases both tumor burden and metastasis in CR2-TAg mice

In a pilot experiment, CR2-TAg mice were treated with the oral metalloproteinase inhibitor AG3340 that potently inhibits MMP-2, -3, -9, -13 and -14 (picomolar IC50 values) and inhibits other MMPs less well (e.g., MMP-1, MMP-7) (22,28). Mice were given AG3340 (n=5) or placebo control (n=4) in their drinking water beginning at six weeks after birth until 24 weeks. Two of the control mice died before 24 weeks, giving a median survival of 164 days (data not shown). In contrast, all AG3340-treated CR2-TAg mice survived to 24 weeks.

AG3340-treated transgenic mice had significantly reduced tumor burdens at 24 weeks compared to the control vehicle-treated mice (p= 0.02; Mann-Whitney test) or to wild type untreated CR2-TAg mice (p=0.0004; Mann-Whitney test) (Fig. 2A). AG3340-treated mice had no macromets to the lung or liver (data not shown), whereas 38% of the untreated mice had macromets to the liver and 14% had macromets to the lung (Supplemental Table 5). Prostate samples from AG3340-treated mice (n=5) were less invasive with a more glandular morphology, whereas control prostates predominantly had invasive carcinoma (Fig. 2B, Supplemental Table 2). Treated tissues had reduced levels of stromal CD45+ cells (Supplementary Fig. 1). AG3340-treated mice still developed small invasive foci with characteristic neuroendocrine rosette patterning and had small carcinomas. We concluded that AG3340 treatment limits but does not prevent neuroendocrine carcinoma progression.

MMP-2 deficiency increases survival

We bred CR2-TAg animals to mice deficient for MMP genes to determine the contributions of specific MMPs to tumor progression. MMP-2- deficient CR2-TAg mice (CR2-TAg;MMP-$2^{-/-}$) had increased survival with a median survival of 201 days (*n*=39) as compared to 188 days for transgenic mice homozygous for the wildtype MMP-2 allele (CR2-TAg;MMP-$2^{+/+}$; *n*=52; p=0.0007; Logrank test) or 188 days for heterozygotes (CR2-TAg;MMP-$2^{+/-}$) (*n*=71; p=0.001) (Figure 2C, Supplemental Table 2).

The lack of MMP-7 or MMP-9 did not impact survival (Supplemental Fig. 2). CR2-TAg;MMP-$7^{-/-}$ animals had a median survival of 173 days (*n*=27), similar to CR2-TAg;MMP-$7^{+/-}$ cohort mice (169 days; *n*=14; p=0.81). CR2-TAg;MMP-$9^{-/-}$ mice had a median

survival of 170 days (*n*=26), which was similar to 171 days for CR2-TAg;MMP-9$^{+/-}$ mice (*n*=52; p=0.75).

MMP-2 contributes to tumor burden

The increased survival in CR2-TAg;MMP-2$^{-/-}$ mice was related to reduced tumorigenicity (Fig. 2A, Supplemental Table 4). Median tumor weights in CR2-TAg;MMP-2$^{-/-}$ mice were significantly lower (0.33 g) than in CR2-TAg;MMP-2$^{+/+}$ mice (2.19 g; p<0.0001; Mann-Whitney test) or CR2-TAg;MMP-2$^{+/-}$ mice (1.11 g; p=0.002). The median tumor weights in CR2-TAg;MMP-2$^{+/-}$ mice were also significantly lower than in the CR2-TAg;MMP-2$^{+/+}$ mice (1.11 g versus 2.19 g, respectively; p=0.04), suggesting that MMP-2 dosage may contribute to tumor burden. In contrast, CR2-TAg;MMP-7$^{-/-}$ and CR2-TAg;MMP-9$^{-/-}$ mice did not show significantly reduced tumor burdens compared to their heterozygous controls (p=0.73 and p=0.15, respectively) (Supplemental Fig. 2).

MMP-2 and -9 contribute differently to glandular and invasive status during tumor progression

We next characterized a cohort of CR2-TAg;MMP-9$^{-/-}$ and CR2-TAg;MMP-9$^{+/-}$ mice at 16 weeks of age using morphometric analysis of prostate sections. CR2-TAg;MMP-9$^{-/-}$ mice (n=6) had a significant increase in the percentage of glands with invasive foci compared to the CR2-TAg;MMP-9$^{+/-}$ controls (n=5; p=0.01; Student's t test) (Fig. 2C). Therefore, in the absence of MMP-9, invasive carcinoma induced by CR2-Tag is accelerated. However, this difference did not alter the survival curve (Supplemental Fig. 2).

CR2-TAg;MMP-7$^{-/-}$ and CR2-TAg;MMP-9$^{-/-}$ tumors were predominantly invasive carcinomas, resembling advanced neuroendocrine tumors with little or no normal glandular tissue (Supplemental Table 1, Fig. 2B).

Compared to the MMP-7 and -9 deficient mice, the CR2-TAg;MMP-2$^{-/-}$ mice had less invasive carcinoma than CR2-TAg;MMP-2$^{+/+}$ mice (Fig. 2B). Similar to the AG3340-treated transgenic mice, the CR2-TAg;MMP-2$^{-/-}$ mice had numerous glands containing high grade PIN. In contrast, MMP-7 and MMP-9 deficient transgenic mice had predominantly carcinoma and invasive phenotypes at 24 weeks, similar to their heterozygous MMP control cohorts (Supplemental Table 1).

MMP-2 decreases lung metastasis

We analyzed lung and liver tissues for metastasic nodule formation at 24 weeks and scored for visible nodules (macromets). H&E stained tissue sections were also analyzed by microscopy for smaller neoplastic nodules (micromets). The percentage of CR2-TAg;MMP-2$^{-/-}$ mice with lung metastases was significantly reduced compared to the MMP-2$^{+/+}$ transgenic animals (p=0.01; Fisher's exact test), with a trend towards reduction in percentage of mice with predominantly micromets (p=0.05) (Figure 3 and Supplemental Table 5).

Although MMP-9 and -7 deficiencies decrease melanoma and lung metastases (32), CR2-TAg;MMP-7$^{-/-}$ mice had no statistically significant difference in metastasis compared to CR2-TAg;MMP-7$^{+/-}$ controls (for lung, p=0.64; for liver, p=1). CR2-TAg;MMP-9$^{-/-}$ mice also showed no difference in the percentage of mice with metastasis compared to CR2-TAg;MMP-9$^{+/-}$ mice (for lung, p=1; for liver, p=0.54).

Proliferation and apoptosis in carcinoma regions of CR2-Tag tumors

To determine if proliferation or apoptosis contributed to reducing tumor burden in the MMP-2$^{-/-}$ mice, we stained tumor sections from 24-week-old animals with anti-phospho-histone H3 (mitotic proliferation marker) and anti-cleaved caspase-3 (apoptosis marker) and

counted positively stained cells per carcinoma region per mouse (Supplemental Fig. 4). There was no significant difference in phospho-histone H3 staining across the different genetic backgrounds, suggesting that there is no difference in proliferation rate within the tumor region (p=0.54; one-way ANOVA).

We detected no significant difference in cleaved caspase-3 staining except in AG3340-treated 24 week old CR2-TAg animals, which had significantly reduced cleaved caspase-3 staining, as compared to the untreated transgenic control (p=0.04; Student's t test) but not compared to the wild type control (p=0.09).

MMPs contribute to increased vasculature in CR2-TAg tumors

Since MMPs are known regulators of vascular density, permeability, and angiogenesis, we investigated the changes in vasculature. In CR2-TAg transgenic mice, blood vessels, as demonstrated by CD31-immunostaining, were present primarily in the peripheral stroma up until 12 weeks of age, but at 16 and 24 weeks tumors were well vascularized (data not shown, Supplemental Fig. 5).

We analyzed the vasculature in MMP deficient mice to determine MMP contribution. At 24 weeks of age, tumors in CR2-TAg; MMP-2$^{-/-}$ mice had reduced numbers of CD31^{+} blood vessels (p=0.01, Student's t test) but not in the number of mature (CD31^{+}SMA^{+}) vessels (p=0.16) (Fig. 4).

By comparison, tumors of CR2-TAg; MMP-7$^{-/-}$ mice at 24 weeks of age had decreased blood vessel size (p=0.02) and reduced endothelial area (p=0.046), but similar vessel density as compared to control heterozygous mouse tumors (Fig. 5, Supplemental Fig. 2). The tumor vessels in the control cohort varied in size and included hyperdilated, irregularly shaped vessels, whereas MMP-7 deficient vessels were more regularly shaped and smaller (Fig. 5).

Previous studies in glioblastoma show that MMP-9 deficient tumor cells are highly invasive and invade perivascularly (33). At 24 weeks of age, CR2-TAg;MMP-9$^{-/-}$ tumor cells showed tumor stromal invasion that had an increased representation of perivascular invasion and a decrease in infiltrative invasion. Heterozygous control tumors had comparatively more vasculature-independent stromal invasion of tumor cells (Fig. 6).

At 24 weeks of age, CR2-TAg;MMP-9$^{-/-}$ mice had similar numbers of vessels within the tumor but decreased vessel size compared to heterozygous controls (Fig. 6 and data not shown). Tumors from the heterozygous control mice had hyperdilated, irregularly shaped vessels, whereas the vasculature within the MMP-9 deficient tumors was more elongated, thin, and regularly shaped. These tissues also showed a reduction in stromal CD45^{+} cells (Supplementary Fig. 1).

Taken together these data suggest that MMP-2 promotes neovascularization of immature blood vessels and MMP-7 increases blood vessel size without an impact on tumor burden. MMP-9 also increases vessel size, reduces the rate of focal invasion of glandular epithelium and promotes vasculature-independent infiltrative invasion.

Discussion

Here we used optical imaging, MMP inhibition, and genetic approaches to determine the role of three MMPs in an aggressive, highly penetrant metastatic tumor model of neuroendocrine origin (Supplemental Table 6). Differential localization and microenvironmental cues contribute to activation and substrate selection of MMPs and other proteases. Clearly, MMP-2,

-7 and -9 have different functions in tumorigenesis in the CR2-TAg neuroendocrine prostate cancer model.

MMP-2 has been implicated in survival, angiogenesis, and metastasis in studies using several tumor models (34-36). Here we demonstrate that MMP-2 is a strong contributor to prostate carcinogenesis. We found that MMP-2 deficiency results in a reduction of immature blood vessel number, which likely contributes to the reduced tumor burden in these mice since neovascularization is necessary to support tumor growth. Previous studies showed MMP-2 has a role in angiogenesis: MMP-2 deficiency decreased corneal angiogenesis (37). Also, in a glioblastoma model, MMP-$2^{-/-}$ had increased survival, increased vessel density, and increased invasive phenotype, migrating along blood vessels in the brain parenchyma (34). However, this vasculature was not functional due to decreased pericyte coverage.

We observed that MMP-7 and MMP-9 contribute to tumor progression, even though they did not impact survival or metastasis in CR2-TAg mice. Previous studies found different roles for MMP-7 in angiogenesis and invasion. Corneal deficiency in MMP-7 leads to increased endothelial area coverage (38). Also overexpressed MMP-7 in prostate cells leads to increased invasion of neighboring tissue (31).

While MMP-9 contributed to vascular remodeling in our model, these aggressive tumors still were able to adapt to its absence and the resulting reduced angiogenesis by increasing perivascular invasion along a more normal vasculature, as we observed previously in glioma (33). Ultimately the MMP-9 deficient tumors developed similar survival and both tumor and metastatic burdens compared to controls. Thus, the same MMP has quite different outcomes in different tumors. How is this regulated? In a number of tumor models, MMP-9 deficiency causes a reduction in tumor progression and metastasis (10). In this study, by 24 weeks, MMP-9 deficiency les to an increased dependence on perivascular invasion and a reduction in vasculature-independent invasion. Whether MMP-9 has pro- or anti-tumorigenic effects depends on the environment and stage in tumor progression. For example, in neuroblastoma and in orthotopically injected pancreatic human cancer cells, loss of MMP-9 results in decreased microvessel size and decreased vascularization (39,40), and in a skin cancer model, MMP-$9^{-/-}$ reduces the number of tumors but increases the malignancy of the tumors formed (41).

MMP-9's role may be determined by the balance between the recruitment of myeloid cells, release of angiogenic factors, and promotion of invasion in a given microenvironment. For example, MMP-9 triggers the release of matrix-bound VEGF in the RIP-TAg model (42). Also, recruitment of bone marrow-derived cells to the tumor stroma and vasculature is MMP-9 dependent in neuroblastoma and other tumor models (43,44). Similarly we saw a reduction in $CD45^{+}$ cells found in the stroma surrounding the tumor. Loss of MMP-9 can delay the angiogenic switch and transition to malignancy, as is the case when macrophage infiltration is prevented in the MMTV-PyMT breast cancer (45). Future studies will be necessary to determine the role, if any, of myeloid cells to these phenotypes.

The response of individual MMPs in the CR2-TAg microenvironment is a balancing act between the substrates and cofactors unique to that tissue. Overlapping substrates could account for a certain amount of MMP redundancy. For example, MMP-2 may be able to compensate for MMP-$9^{-/-}$. We detected increased expression of MMP-2, -7, and -9 following treatment with AG3340, as has been seen previously using other MMP inhibitors (Supplemental Fig. 3) (46-48). Interestingly, in glioblastoma, MMP-2 and MMP-9 deficiency stimulates perivascular invasion, similar to our observations seen here following MMP-9 deficiency (33, 34). Also, strain-dependent variances account for some variation between genotypes in breast cancer studies and may play a role in humans (49).

We exploited the CR2-TAg animal model for characterizing MMP genes and identifying potential therapeutic treatments of aggressive neuroendocrine malignancies. We found that treatment with the MMP inhibitor AG3340 decreased tumor burden and slowed tumor progression. Similarly, AG3340 treatment of a neuroblastoma tumor progression model increases survival and reduced tumor burden, lung metastasis, and microvessel size (39). Since AG3340 is a strong inhibitor of tumorigenesis when given to the mouse early in tumor progression, an MMP inhibitor such as AG3340 may have therapeutic efficacy in certain forms of prostate cancer, although we predict it would be insufficient to result in complete tumor ablation, since here the tumor adapted to the microenvironment and became invasive.

Based on our study, therapeutic use of broad spectrum MMP inhibitors may have unpredictable results, possibly even a more invasive tumor pathology, which has been seen in some human studies (50). Targeting MMPs does not seem to stop tumor progression of late, highly aggressive tumors. Cleverly, the tumors progress aggressively through alternative routes. Thus, treatment of the most aggressive tumors will require similarly aggressive multi-hit therapies. Combination therapies including selective MMP inhibition may be of therapeutic benefit for the most aggressive prostate malignancies with neuroendocrine features or other types of neuroendocrine tumors.

Supplementary Material

Refer to Web version on PubMed Central for supplementary material.

Acknowledgments

Grant support: This study was supported by grants to Z.W. (CA072006) and a Development project from the UCSF Prostate SPORE (CA089520), American Cancer Society Postdoctoral Fellowship (L.L.), Ruth L. Kirschstein National Research Service Award (CA103534) (L.L.), Career Development award from the Bay Area Breast SPORE (CA58207) (M.S.), and K08 Award (NS063456) (J.P.).

We thank David Shalinsky (Agouron) for the MMP inhibitor AG3340, Doug Hanahan for the SV40-TAg antibody, and Lynn Matrisian for the MMP-7 knockout mice and antibody. Special thanks to Elena Atamaniuc and Bernard Thompson (T.W.) for mouse care, Helen Capili for tissue sectioning, and the Werb lab for helpful discussions.

References

1. Jemal A, Siegel R, Ward E, Hao Y, Xu J, Thun MJ. Cancer statistics, 2009. CA Cancer J Clin 2009;59 (4):225–49. [PubMed: 19474385]
2. Turbat-Herrera EA, Herrera GA, Gore I, Lott RL, Grizzle WE, Bonnin JM. Neuroendocrine differentiation in prostatic carcinomas. A retrospective autopsy study. Arch Pathol Lab Med 1988;112 (11):1100–5. [PubMed: 2460064]
3. Vashchenko N, Abrahamsson PA. Neuroendocrine differentiation in prostate cancer: implications for new treatment modalities. Eur Urol 2005;47(2):147–55. [PubMed: 15661408]
4. Komiya A, Suzuki H, Imamoto T, et al. Neuroendocrine differentiation in the progression of prostate cancer. Int J Urol 2009;16(1):37–44. [PubMed: 19120524]
5. Bonkhoff H, Stein U, Remberger K. Androgen receptor status in endocrine-paracrine cell types of the normal, hyperplastic, and neoplastic human prostate. Virchows Arch A Pathol Anat Histopathol 1993;423(4):291–4. [PubMed: 7694424]
6. di Sant'Agnese PA. Neuroendocrine differentiation in prostatic carcinoma: an update on recent developments. Ann Oncol 2001;12:S135–40. [PubMed: 11762341]
7. Abrahamsson PA. Neuroendocrine differentiation in prostatic carcinoma. Prostate 1999;39(2):135–48. [PubMed: 10221570]
8. Garabedian EM, Roberts LJ, McNevin MS, Gordon JI. Examining the role of Paneth cells in the small intestine by lineage ablation in transgenic mice. J Biol Chem 1997;272(38):23729–40. [PubMed: 9295317]

9. Garabedian EM, Humphrey PA, Gordon JI. A transgenic mouse model of metastatic prostate cancer originating from neuroendocrine cells. Proc Natl Acad Sci U S A 1998;95(26):15382–7. [PubMed: 9860977]
10. Egeblad M, Werb Z. New functions for the matrix metalloproteinases in cancer progression. Nat Rev Cancer 2002;2(3):161–74. [PubMed: 11990853]
11. Sternlicht MD, Werb Z. How matrix metalloproteinases regulate cell behavior. Annu Rev Cell Dev Biol 2001;17:463–516. [PubMed: 11687497]
12. Lokeshwar BL. MMP inhibition in prostate cancer. Ann N Y Acad Sci 1999;878:271–89. [PubMed: 10415736]
13. Wood M, Fudge K, Mohler JL, et al. In situ hybridization studies of metalloproteinases 2 and 9 and TIMP-1 and TIMP-2 expression in human prostate cancer. Clin Exp Metastasis 1997;15(3):246–58. [PubMed: 9174126]
14. Knox JD, Wolf C, McDaniel K, et al. Matrilysin expression in human prostate carcinoma. Mol Carcinog 1996;15(1):57–63. [PubMed: 8561867]
15. Pajouh MS, Nagle RB, Breathnach R, Finch JS, Brawer MK, Bowden GT. Expression of metalloproteinase genes in human prostate cancer. J Cancer Res Clin Oncol 1991;117(2):144–50. [PubMed: 1848860]
16. Trudel D, Fradet Y, Meyer F, Harel F, Tetu B. Significance of MMP-2 expression in prostate cancer: an immunohistochemical study. Cancer Res 2003;63(23):8511–5. [PubMed: 14679018]
17. Rabbani SA, Harakidas P, Guo Y, Steinman D, Davidsen SK, Morgan DW. Synthetic inhibitor of matrix metalloproteases decreases tumor growth and metastases in a syngeneic model of rat prostate cancer in vivo. Int J Cancer 2000;87(2):276–82. [PubMed: 10861487]
18. Sehgal G, Hua J, Bernhard EJ, Sehgal I, Thompson TC, Muschel RJ. Requirement for matrix metalloproteinase-9 (gelatinase B) expression in metastasis by murine prostate carcinoma. Am J Pathol 1998;152(2):591–6. [PubMed: 9466586]
19. Itoh T, Ikeda T, Gomi H, Nakao S, Suzuki T, Itohara S. Unaltered secretion of beta-amyloid precursor protein in gelatinase A (matrix metalloproteinase 2)-deficient mice. J Biol Chem 1997;272(36): 22389–92. [PubMed: 9278386]
20. Wilson CL, Heppner KJ, Labosky PA, Hogan BL, Matrisian LM. Intestinal tumorigenesis is suppressed in mice lacking the metalloproteinase matrilysin. Proc Natl Acad Sci U S A 1997;94(4): 1402–7. [PubMed: 9037065]
21. Vu TH, Shipley JM, Bergers G, et al. MMP-9/gelatinase B is a key regulator of growth plate angiogenesis and apoptosis of hypertrophic chondrocytes. Cell 1998;93(3):411–22. [PubMed: 9590175]
22. Bremer C, Tung CH, Weissleder R. In vivo molecular target assessment of matrix metalloproteinase inhibition. Nat Med 2001;7(6):743–8. [PubMed: 11385514]
23. Ntziachristos V, Tung CH, Bremer C, Weissleder R. Fluorescence molecular tomography resolves protease activity in vivo. Nat Med 2002;8(7):757–60. [PubMed: 12091907]
24. Herron GS, Banda MJ, Clark EJ, Gavrilovic J, Werb Z. Secretion of metalloproteinases by stimulated capillary endothelial cells. II. Expression of collagenase and stromelysin activities is regulated by endogenous inhibitors. J Biol Chem 1986;261(6):2814–8. [PubMed: 3005266]
25. Fingleton B, Powell WC, Crawford HC, Couchman JR, Matrisian LM. A rat monoclonal antibody that recognizes pro- and active MMP-7 indicates polarized expression in vivo. Hybridoma (Larchmt) 2007;26(1):22–7. [PubMed: 17316082]
26. Behrendtsen O, Alexander CM, Werb Z. Metalloproteinases mediate extracellular matrix degradation by cells from mouse blastocyst outgrowths. Development 1992;114(2):447–56. [PubMed: 1317291]
27. Shappell SB, Thomas GV, Roberts RL, et al. Prostate pathology of genetically engineered mice: definitions and classification. The consensus report from the Bar Harbor meeting of the Mouse Models of Human Cancer Consortium Prostate Pathology Committee. Cancer Res 2004;64(6):2270–305. [PubMed: 15026373]
28. Shalinsky DR, Brekken J, Zou H, et al. Broad antitumor and antiangiogenic activities of AG3340, a potent and selective MMP inhibitor undergoing advanced oncology clinical trials. Ann N Y Acad Sci 1999;878:236–70. [PubMed: 10415735]

29. Condon MS, Bosland MC. The role of stromal cells in prostate cancer development and progression. In Vivo 1999;13(1):61–5. [PubMed: 10218135]
30. Olumi AF, Grossfeld GD, Hayward SW, Carroll PR, Tlsty TD, Cunha GR. Carcinoma-associated fibroblasts direct tumor progression of initiated human prostatic epithelium. Cancer Res 1999;59 (19):5002–11. [PubMed: 10519415]
31. Powell WC, Domann FE Jr, Mitchen JM, Matrisian LM, Nagle RB, Bowden GT. Matrilysin expression in the involuting rat ventral prostate. Prostate 1996;29(3):159–68. [PubMed: 8827084]
32. Itoh T, Tanioka M, Matsuda H, et al. Experimental metastasis is suppressed in MMP-9-deficient mice. Clin Exp Metastasis 1999;17(2):177–81. [PubMed: 10411111]
33. Du R, Lu KV, Petritsch C, et al. HIF1alpha induces the recruitment of bone marrow-derived vascular modulatory cells to regulate tumor angiogenesis and invasion. Cancer Cell 2008;13(3):206–20. [PubMed: 18328425]
34. Du R, Petritsch C, Lu K, et al. Matrix metalloproteinase-2 regulates vascular patterning and growth affecting tumor cell survival and invasion in GBM. Neuro Oncol 2008;10(3):254–64. [PubMed: 18359864]
35. Ohno-Matsui K, Uetama T, Yoshida T, et al. Reduced retinal angiogenesis in MMP-2-deficient mice. Invest Ophthalmol Vis Sci 2003;44(12):5370–5. [PubMed: 14638740]
36. Itoh T, Tanioka M, Yoshida H, Yoshioka T, Nishimoto H, Itohara S. Reduced angiogenesis and tumor progression in gelatinase A-deficient mice. Cancer Res 1998;58(5):1048–51. [PubMed: 9500469]
37. Kato T, Kure T, Chang JH, et al. Diminished corneal angiogenesis in gelatinase A-deficient mice. FEBS Lett 2001;508(2):187–90. [PubMed: 11718713]
38. Kure T, Chang JH, Kato T, et al. Corneal neovascularization after excimer keratectomy wounds in matrilysin-deficient mice. Invest Ophthalmol Vis Sci 2003;44(1):137–44. [PubMed: 12506066]
39. Chantrain CF, Shimada H, Jodele S, et al. Stromal matrix metalloproteinase-9 regulates the vascular architecture in neuroblastoma by promoting pericyte recruitment. Cancer Res 2004;64(5):1675–86. [PubMed: 14996727]
40. Nakamura T, Kuwai T, Kim JS, Fan D, Kim SJ, Fidler IJ. Stromal metalloproteinase-9 is essential to angiogenesis and progressive growth of orthotopic human pancreatic cancer in parabiont nude mice. Neoplasia 2007;9(11):979–86. [PubMed: 18030366]
41. Coussens LM, Tinkle CL, Hanahan D, Werb Z. MMP-9 supplied by bone marrow-derived cells contributes to skin carcinogenesis. Cell 2000;103(3):481–90. [PubMed: 11081634]
42. Bergers G, Brekken R, McMahon G, et al. Matrix metalloproteinase-9 triggers the angiogenic switch during carcinogenesis. Nat Cell Biol 2000;2(10):737–44. [PubMed: 11025665]
43. Jodele S, Chantrain CF, Blavier L, et al. The contribution of bone marrow-derived cells to the tumor vasculature in neuroblastoma is matrix metalloproteinase-9 dependent. Cancer Res 2005;65(8): 3200–8. [PubMed: 15833851]
44. Ahn GO, Brown JM. Matrix metalloproteinase-9 is required for tumor vasculogenesis but not for angiogenesis: role of bone marrow-derived myelomonocytic cells. Cancer Cell 2008;13(3):193–205. [PubMed: 18328424]
45. Lin EY, Li JF, Gnatovskiy L, et al. Macrophages regulate the angiogenic switch in a mouse model of breast cancer. Cancer Res 2006;66(23):11238–46. [PubMed: 17114237]
46. Kruger A, Soeltl R, Sopov I, et al. Hydroxamate-type matrix metalloproteinase inhibitor batimastat promotes liver metastasis. Cancer Res 2001;61(4):1272–5. [PubMed: 11245418]
47. Almholt K, Juncker-Jensen A, Laerum OD, et al. Metastasis is strongly reduced by the matrix metalloproteinase inhibitor Galardin in the MMTV-PymT transgenic breast cancer model. Mol Cancer Ther 2008;7(9):2758–67. [PubMed: 18790756]
48. Lund LR, Romer J, Bugge TH, et al. Functional overlap between two classes of matrix-degrading proteases in wound healing. Embo J 1999;18(17):4645–56. [PubMed: 10469644]
49. Martin MD, Carter KJ, Jean-Philippe SR, et al. Effect of ablation or inhibition of stromal matrix metalloproteinase-9 on lung metastasis in a breast cancer model is dependent on genetic background. Cancer Res 2008;68(15):6251–9. [PubMed: 18676849]
50. Coussens LM, Fingleton B, Matrisian LM. Matrix metalloproteinase inhibitors and cancer: trials and tribulations. Science 2002;295(5564):2387–92. [PubMed: 11923519]

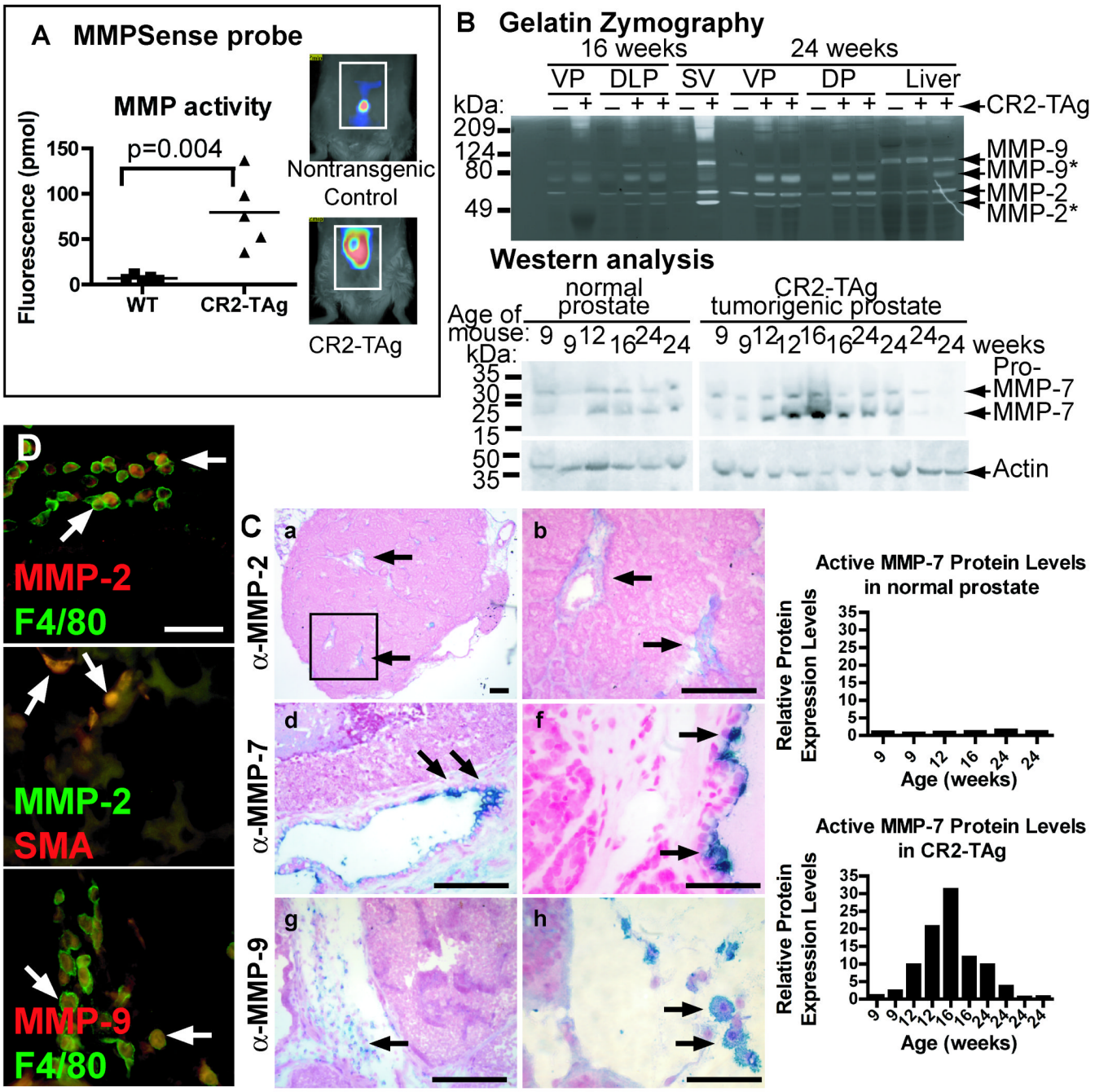

Figure 1. MMP activity and localization in normal prostate and CR2-TAg tumors

A, Detected fluorescence (pmol) following activation of MMPSense probe using tomography. *B*, Gelatin zymography of ventral and dorsolateral prostates, seminal vesicle, and liver collected from CR2-TAg transgenic mice and normal littermates at 16 and 24 weeks. Western blot analysis of MMP-7 activity in normal prostate and CR2-TAg tumorigenic prostate over time. Samples were collected at 9, 12, 16 and 24 weeks. Graphs represent the expression of MMP-7 normalized to actin staining. *C*, Immunohistochemistry of MMP-2 *(a-c)*, MMP-7 *(d-f)*, and MMP-9 *(g-i)* in CR2-TAg tumors at 24 weeks of age. *Arrows*, positively stained cells. The box in *a* is enlarged in *b*. D, Co-localization of MMP-2 (red) and F4/80 (green) (top panel), MMP-2 (green) and smooth muscle actin (SMA; red) (middle panel), and MMP-9 and F4/80

(green) (bottom panel) by immunofluorescence in CR2-TAg tumor stroma at 24 weeks. *Scale bars, for C*, 100 μm in *a*, *b*, *d*, *e*, *g*, and *i*; 40 μm in *c*, *f*, and *h; for D, 50* μm.

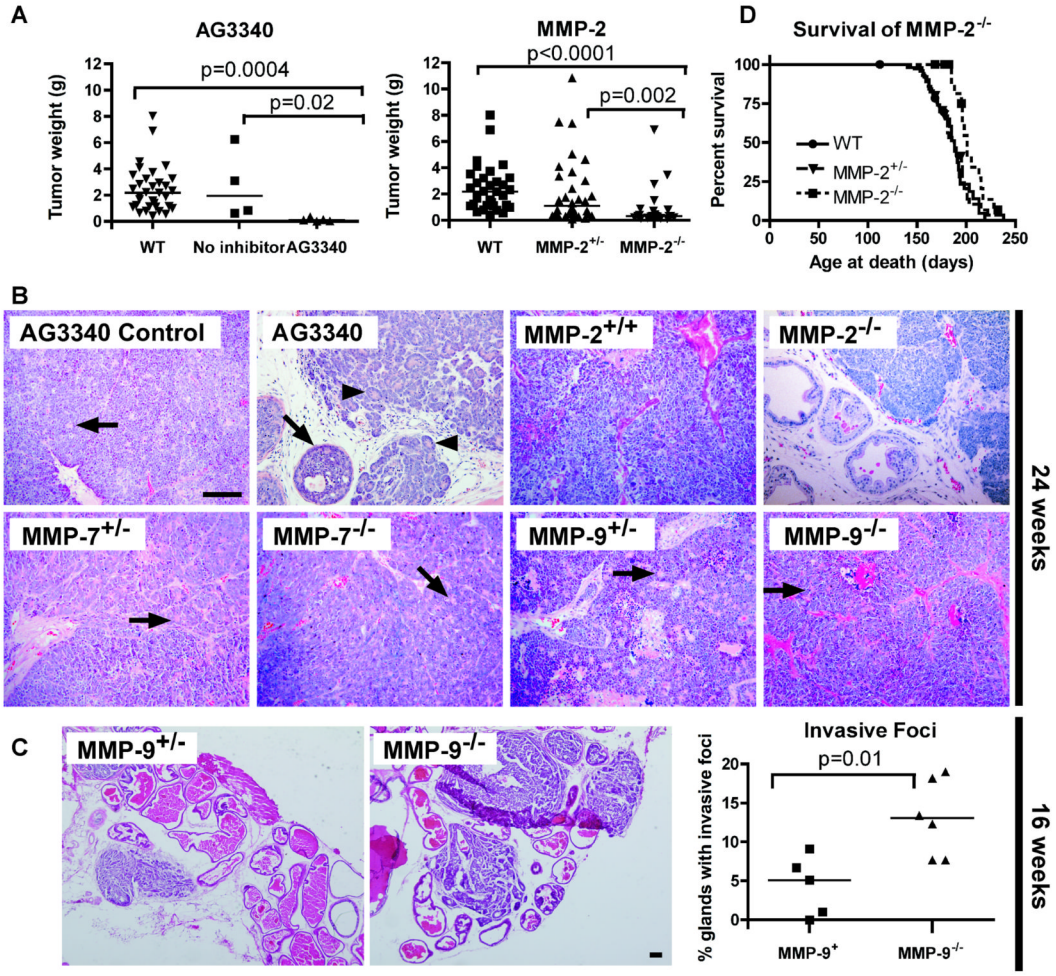

Figure 2. Tumors in CR2-TAg mice deficient for MMPs

A, Left graph, CR2-TAg mice treated with MMP inhibitor AG3340 have decreased tumor weight (grams) compared to uninjected nontransgenic (wild type) mice or to wild type untreated mice. *Shapes*, prostate weight from one mouse. *Lines*, median prostate weight per cohort. *Right graph*, CR2-TAg;MMP-2$^{-/-}$ mice have reduced tumor burden compared to wild type or to heterozygotes. *B*, H&E staining of representative tissue sections from CR2-TAg tumors at 24 weeks. *AG3340 arrow*, high grade PIN; *Arrowheads*, glands. *Other arrows*, neuroendocrine rosettes. *C*, H&Es of CR2-TAg;MMP-9$^{+/-}$ (*left*) and CR2-TAg;MMP-9$^{-/-}$ (*right*) at 16 weeks. *Graph*, Quantification of invasive foci as a percentage of total number of glands per section. *D*, Survival curve for CR2-TAg;MMP-2$^{-/-}$ mice. MMP-2 deficient mice have delayed survival compared to wild type. *Shapes*, censored subjects.

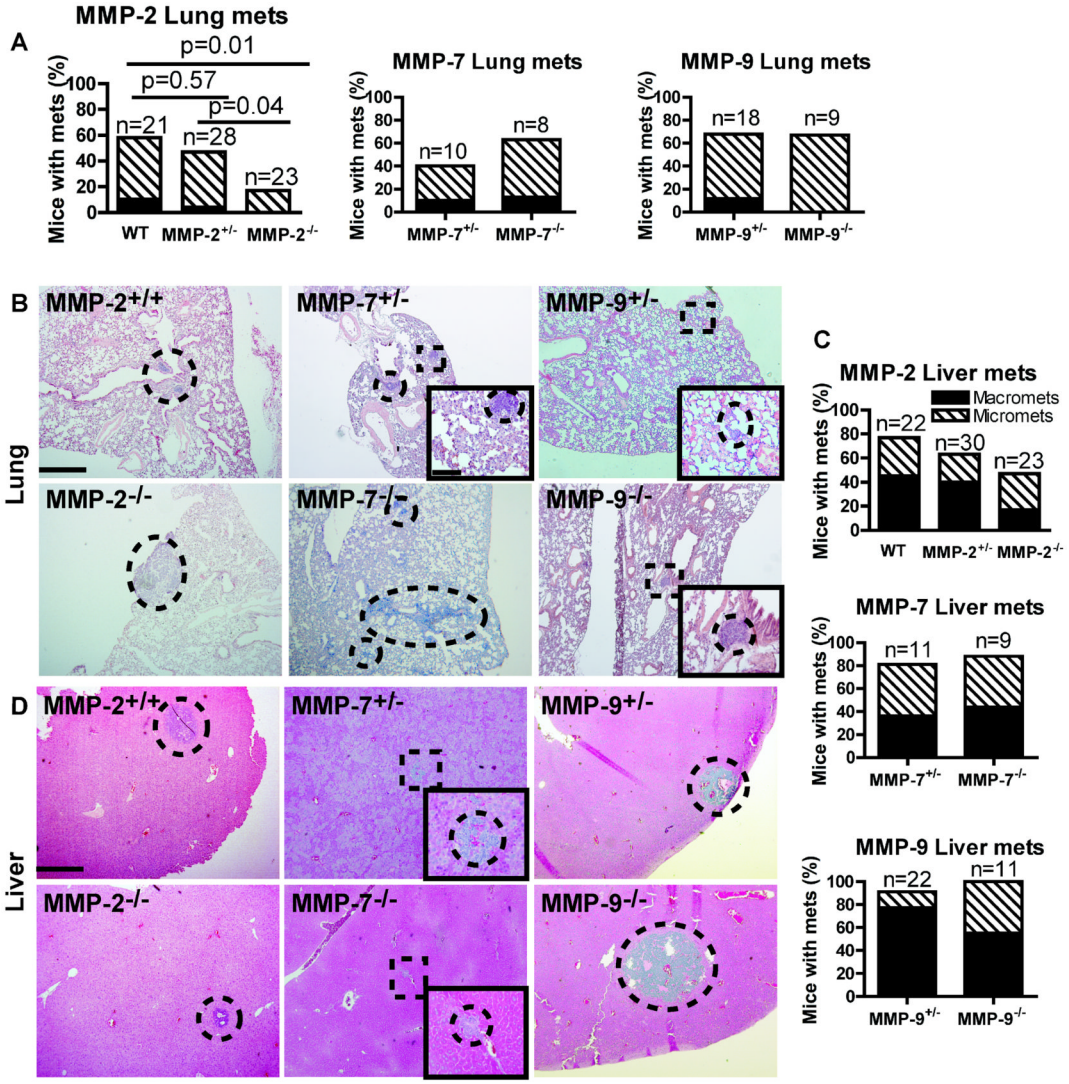

Figure 3. Metastasis to lung and liver in MMP deficient backgrounds

A, Graphs of percentage of mice that have macro (solid black) or micro (stripes) metastases to the lung in CR2-TAg mice deficient for MMP-2, -7, and -9. *B*, Representative lung metastases in CR2-TAg mice with the indicated MMP deficiencies. *C*, Graphs of percentage of mice that have macro or micro metastases to the liver in CR2-TAg mice deficient for MMP-2, -7, and -9. *D*, Pictures of representative liver metastases in CR2-TAg mice with the indicated MMP deficiencies. *Dotted lines*, metastatic nodules within lung and liver tissue harvested from animals of the indicated genotype. *Squares with dotted lines*, regions enlarged in insets. *Scale bars*, 500 μm for MMP-$2^{+/+}$ and 100 μm for inserts.

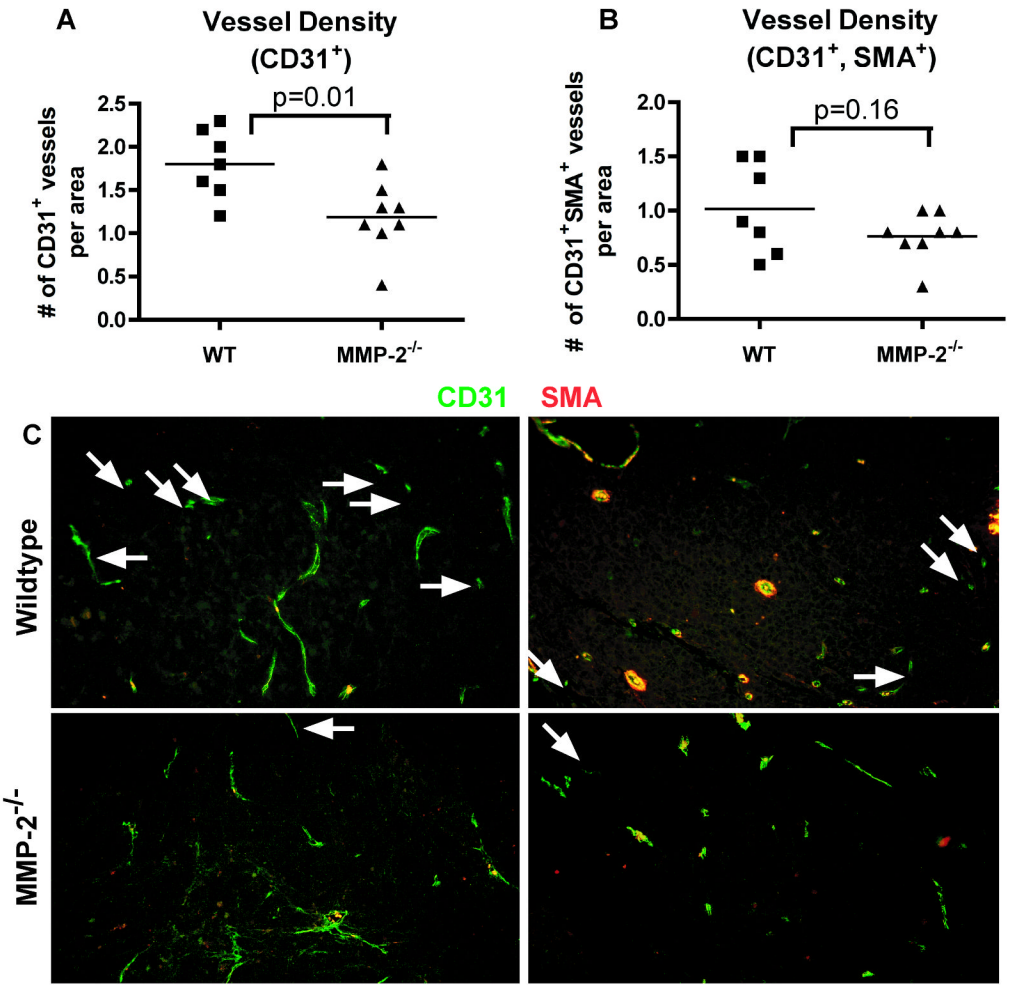

Figure 4. Mice deficient for MMP-2 have decreased blood vessel density in tumor regions

Tissues from mice with the indicated genotypes were collected at 24 weeks and stained by immunofluorescence with markers of vasculature (CD31) and pericytes (SMA) and analyzed by morphometric analysis. *A*, Quantification of vessel density based on immunofluorescence staining using CD31 antibodies. MMP-2 deficient tumors have reduced vessel density (number of $CD31^+$ vessels per 100,000 pixels). *B*, Quantification of mature vessel density ($CD31^+SMA^+$) based on immunofluorescence staining using CD31 and smooth muscle actin (SMA) antibodies. *C*, Immunofluorescence of vessels stained with antibodies to CD31 (*green*) and SMA (*red*) in tumors from CR2-TAg;MMP-$2^{+/+}$ (*top row*) and CR2-TAg;MMP-$2^{-/-}$ (*bottom row*) prostate tumors. *Arrows*: $CD31^+SMA^-$ vessels. *Scale bar: 100 μm.*

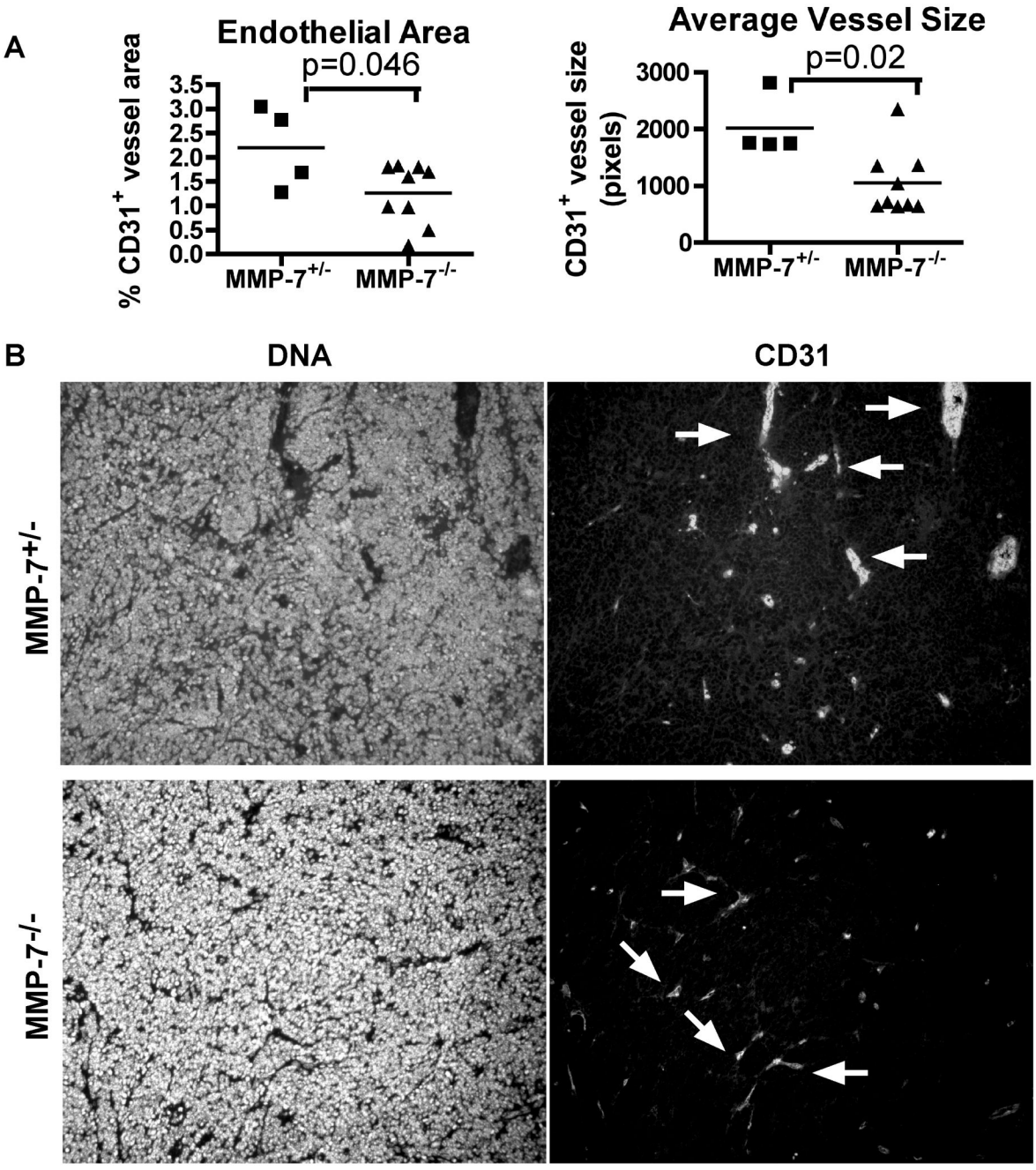

Figure 5. CR2-Tag mice deficient for MMP-7 have decreased endothelial area and decreased vessel size in regions of the prostate with tumor

Tissues from mice with the indicated genotypes were collected at 24 weeks, stained by immunofluorescence with markers of endothelium (CD31) and pericytes (SMA), and scored within the tumor region by morphometric analysis. *Shapes*, one per mouse, *Line*, mean. *A*, Quantification of vessel density ($CD31^+$ per 100,000 pixels). Quantification of mature vessel density ($CD31^+SMA^+$ per 100,000 pixels). Quantification of endothelial area in MMP-7 deficient mice. Quantification of average size of $CD31^+$ vessels (pixels). *B*, Immunofluorescence of vessels stained with Hoechst (left two panels) and CD31 (right two

panels) in tumors from CR2-TAg;MMP-$7^{+/-}$ (upper two panels) or CR2-TAg;MMP-$7^{-/-}$. *Arrows*, $CD31^{+}$ vessels.

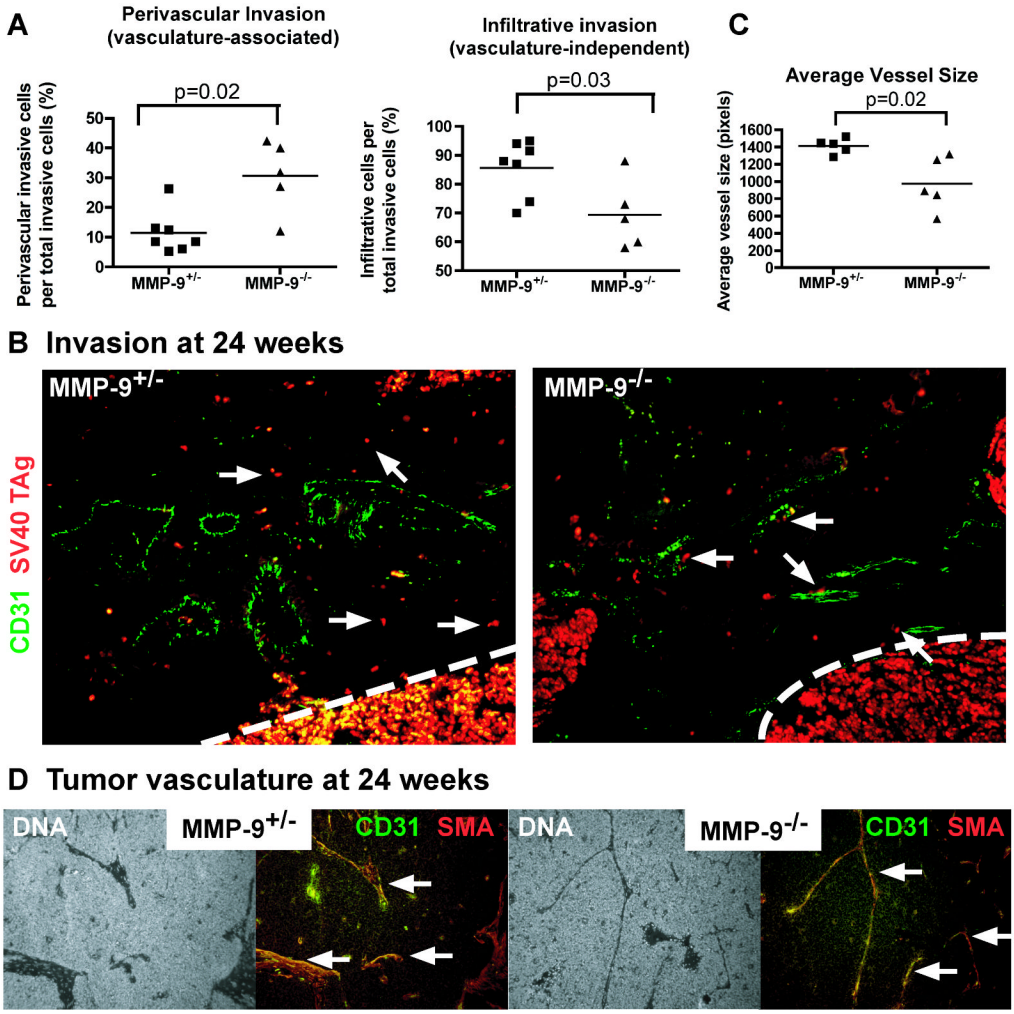

Figure 6. Mice deficient for MMP-9 have increased perivascular invasion, increased stromal vasculature density, and decreased vessel size in tumor regions

A, Quantification of infiltrative and perivascular invasion at 24 weeks of age. Tumor cells escaped from the tumor into the stroma were scored as cells that were (perivascular) or were not (infiltrative) associated with the vasculature. *Shapes*, one per mouse. *Line*, mean. *B*, Immunofluorescence staining of tumor cells and blood vessels at tumor-stroma border at 24 weeks using SV40 TAg (*red*) and CD31 (*green*) antibodies, respectively. *Arrows*, tumor cells not associated with vessels (*left image*, CR2-TAg;MMP-$9^{+/-}$) or associated with vessels (*right image*, CR2-Tag;MMP-$9^{-/-}$). *C*, Quantification of average vessel size of $CD31^{+}$ vessels at 24 weeks. *Line*, mean. MMP-9 deficient tumors have reduced vessel size. *D*, Immunofluorescence staining of tumor vasculature at 24 weeks using CD31 (*green*) and SMA (*red*) antibodies. *Arrows*, vasculature.